PRAMANA — journal of physics

Vol. 78, No. 3
March 2012
pp. 389–398

Fragmentation and momentum correlations in heavy-ion collisions

SAKSHI GAUTAM[1,*] and RAJNI KANT[2]

[1]Department of Physics, Panjab University, Chandigarh 160 014, India
[2]House No. 276, Ward No. 11, Tibbabasti, Patran, Patiala 147 105, India
*Corresponding author. E-mail: sakshigautm@gmail.com

MS received 9 July 2011; revised 17 September 2011; accepted 14 October 2011

Abstract. The role of momentum correlations in the production of light and medium mass fragments is studied by imposing momentum cut in the clusterization of the phase space. Our detailed investigation shows that momentum cut has a major role to play in the emission of fragments. A comparison with the experimental data is also presented. The calculations showed better agreement with the experimental data when momentum cut is imposed.

Keywords. Quantum molecular dynamics; multifragmentation; momentum correlations.

PACS Nos 25.70.Pq; 24.10.Cn; 24.10.Lx

1. Introduction

It is well known that colliding nuclei break into several small and medium size pieces and a lot of nucleons are also emitted. The study of this subfield, known as multifragmentation, gained momentum after several theoretical and experimental groups around the world put their collective efforts to understand this process [1]. Because of the accumulation of experimental data on multifragmentation, one has the opportunity to study the role of dynamical correlations in fragment formation. Theoretically, the availability of a large number of models makes the situation worse [1–4]. As fragmentation needs fluctuations and correlations, the molecular dynamical models are the only resource in theoretical domains. The molecular dynamics (n-body) approach is well suited as it incorporates the correlations and fluctuations among the nucleons. We shall, therefore, use quantum molecular dynamics (QMD) model [2,3] to study the dynamics of heavy-ion collisions. Since every model simulates single nucleon, i.e., gives the phase-space of all the nucleons, to study fragmentation one needs to first clusterize them. In a very simple picture, we can define a cluster using space correlations. This method is known as the minimum spanning tree (MST) method [5]. In this method, we allow nucleons to form a cluster if their centroids are less than 4 fm. This method works fine when the system

DOI: 10.1007/s12043-011-0246-5; ***e*Publication: 16 February 2012**

is very dilute. But, the fragments formed by the MST method will be highly unstable (especially in central collisions) as there the two nucleons may not be well formed and therefore can be unstable and decay after a while. To filter out such unstable fragments, we impose another cut in terms of the relative momentum of nucleons. This method, dubbed as minimum spanning tree with momentum cut (MSTP) method was discussed by Kumar *et al* [6]. Unfortunately, this study was restricted to heavier systems like ^{93}Nb+^{93}Nb and ^{197}Au+^{197}Au reactions. The role of momentum cut on the fragment structure of lighter systems is still unclear. We aim to address this in this paper.

Exclusively, we plan to (i) see the role of momentum cut on the fragment structure of lighter colliding systems and (ii) see the role of colliding geometry on the fragment structure with momentum cut being imposed.

The present study is carried out within the framework of the QMD model [2,3] which is described in the following section.

2. The formalism

2.1 *Quantum molecular dynamics (QMD) model*

We describe the time evolution of a heavy-ion reaction within the framework of quantum molecular dynamics (QMD) model [2,3] which is based on a molecular dynamics picture. This model has been successful in explaining collective flow [7], elliptic flow [8], multifragmentation [9] as well as dense and hot matter [10]. In QMD model, nucleons (represented by Gaussian wave packets) interact via mutual two- and three-body interactions. Here, each nucleon is represented by a coherent state of the form

$$\psi_i(\mathbf{r}, \mathbf{p}_i(t), \mathbf{r}_i(t)) = \frac{1}{(2\pi L)^{3/4}} \exp\left[\frac{i}{\hbar}\mathbf{p}_i(t)\cdot\mathbf{r} - \frac{(\mathbf{r}-\mathbf{r}_i(t))^2}{4L}\right], \tag{1}$$

where L is the width of the Gaussian wave packet and $\mathbf{r}_i(t)$ and $\mathbf{p}_i(t)$ are time-dependent parameters to be determined. The total N-body function is assumed to be a direct product of the coherent states (eq. (1))

$$\Phi = \prod_i \psi_i(\mathbf{r}, \mathbf{r}_i, \mathbf{p}_i, t). \tag{2}$$

By doing this, one neglects the antisymmetrization.

The equations of motion for many-body system are, then, calculated by means of a generalized variational principle. For the coherent states and Hamiltonian of the form $H = \sum_i T_i + \frac{1}{2}\sum_{ij} V_{ij}$ (T_i = kinetic energy and V_{ij} = potential energy), the Lagrangian and the variation can easily be calculated and we obtain

$$\mathcal{L} = \sum_i \left[-\dot{\mathbf{r}}_i\mathbf{p}_i - T_i - \frac{1}{2}\sum_{j\neq i}\langle V_{ij}\rangle - \frac{3}{2Lm}\right], \tag{3}$$

$$\dot{\mathbf{r}}_i = \frac{\mathbf{p}_i}{m} + \nabla_{\mathbf{p}_i}\sum_j \langle V_{ij}\rangle = \nabla_{\mathbf{p}_i}\langle H\rangle, \tag{4}$$

$$\dot{\mathbf{p}}_i = -\nabla_{\mathbf{r}_i}\sum_{j\neq i}\langle V_{ij}\rangle = -\nabla_{\mathbf{r}_i}\langle H\rangle, \tag{5}$$

where, eqs (4) and (5) determine the time-dependent parameters $\mathbf{r}_i(t)$ and $\mathbf{p}_i(t)$, with $\mathbf{r}_i = \mathbf{r}_i + (\mathbf{p}_i/m)t$ and $\langle V_{ij}\rangle = \int \mathrm{d}^3\mathbf{r}_1\mathrm{d}^3\mathbf{p}_2\langle\psi_i^*\psi_j^*|V(\mathbf{r}_1,\mathbf{r}_2)|\psi_i\psi_j\rangle$. These equations represent the time evolution and can be solved numerically. Therefore, the variational principle reduces the time evolution of n-body Schrödinger equation to the time evolution $6\times(A_P + A_T)$ equations. The equations of motion now have a similar structure like the classical Hamiltonian equations

$$\dot{\mathbf{p}}_i = -\frac{\partial\langle H\rangle}{\partial\mathbf{r}_i}; \quad \dot{\mathbf{r}}_i = \frac{\partial\langle H\rangle}{\partial\mathbf{p}_i}. \tag{6}$$

The expectation value of the total Hamiltonian reads as

$$\begin{aligned}\langle H\rangle &= \langle T\rangle + \langle V\rangle \\ &= \sum_i \frac{\mathbf{p}_i^2}{2m_i} + V^{\mathrm{Skyrme}} + V^{\mathrm{Yuk}} + V^{\mathrm{Coul}}.\end{aligned} \tag{7}$$

Here V^{Skyrme}, V^{Yuk} and V^{Coul} are, respectively, the local (two-and three-body) Skyrme, Yukawa and Coulomb potentials. The relativistic effect does not play any role in the low incident energy of the present interest [11].

The phase-space of the nucleons is stored at several time-steps. The QMD model does not give any information about the fragments observed at the final stage of the reaction. In order to construct the fragments, one needs clusterization algorithms. We shall concentrate here on the MST and MSTP methods.

According to MST method [5], two nucleons are allowed to share the same fragment if their centroids are closer than a distance r_{min}, i.e.,

$$|\mathbf{r_i} - \mathbf{r_j}| \leq r_{\mathrm{min}}, \tag{8}$$

where $\mathbf{r_i}$ and $\mathbf{r_j}$ are the spatial positions of both nucleons and r_{min} is taken to be 4 fm.

For MSTP method,we impose an additional cut in the momentum space, i.e., we allow only those nucleons to form a fragment which in addition to eq. (8) also satisfy

$$|\mathbf{p_i} - \mathbf{p_j}| \leq p_{\mathrm{min}}, \tag{9}$$

where p_{min} = 150 MeV/c.

3. Results and discussion

We simulated the reactions of ^{12}C+^{12}C , ^{40}Ca+^{40}Ca, ^{96}Zr+^{96}Zr and ^{197}Au+^{197}Au at 100 and 400 MeV/nucleon at $\hat{b} = b/b_{\mathrm{max}} = 0.0, 0.2, 0.4, 0.6$ and 0.8, where $b_{\mathrm{max}} = R_0(A_{\mathrm{P}}^{1/3} + A_{\mathrm{T}}^{1/3})$ with $R_0 = 1.142$ fm and A_{P} and A_{T} represent the mass of the projectile and target nucleus. We use a soft equation of state with standard energy-dependent Cugnon cross-section [12].

In figure 1, we display the time evolution of A^{max} (figures 1a and 1b), free nucleons (figures 1c and 1d) and LCPs ($2 \leq A \leq 4$) (figures 1e and 1f) for ^{12}C+^{12}C reactions at 100 (left panels) and 400 (right panels) MeV/nucleon for central collisions. Solid lines indicate the results of the MST method whereas dashed lines represent the results of the MSTP method. The heaviest fragment A^{max} follows different time evolutions in MSTP

compared to MST method. Finally, both emerge to similar results. Naturally, at the start of the collision, the colliding nuclei have very large relative momentum and so the MSTP method gives two clusters each having its mass equal to the projectile/target nucleus, whereas in the MST method, one gets a single fragment having mass nearly equal to the combined mass of the projectile and the target nucleus. Also, a cut in relative momentum of nucleons clearly helps in identifying the largest fragment quite early in time. From the figure, one also notices that in the MSTP method, the fragment emission starts at a time when the MST method gives a single big fragment. This is because the MST approach is based on simple spatial correlations. Therefore, in this approach the nucleons with large relative momenta will also be part of a cluster, though MSTP method forbids such nucleons to be in the same cluster.

In figures 1c and 1d, we display the time evolution of free nucleons. We see that for both the energies, MSTP method yields more free nucleons compared to MST method. There is also a delayed emission of nucleons in MST because no restrictions are being imposed on the relative momentum in MST method. This delayed emission of free nucleons in the MST method is due to the fact that until 30 fm/c, we have a single big fragment in MST method (see figures 1a and 1b) and so it will keep on emitting nucleons, whereas in MSTP method, because of the momentum cut we have more bound fragments and so emission of free nucleons will eventually be less as the reaction proceeds. Because of the early emission of fragments and free nucleons in MSTP method, we find that the fragments saturate earlier in MSTP than in MST as predicted in ref. [6].

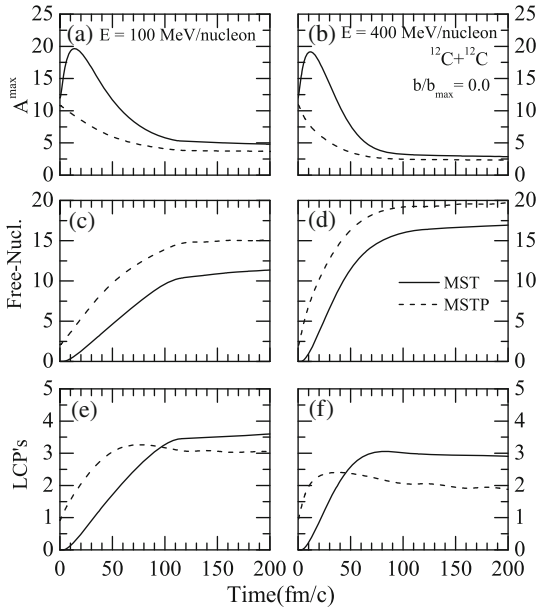

Figure 1. The time evolution of $A^{\max}$, free nucleons and LCPs for the $^{12}C+^{12}C$ reaction at an incident energy of 100 (left panels) and 400 MeV/nucleon (right panels) with MST and MSTP methods, respectively.

In figures 1e and 1f, we display the time evolution of LCPs. We see that the MST method yields more LCPs. The difference between the MST and MSTP methods increases at 400 MeV/nucleon signifying the significant role of momentum correlations at higher incident energies.

In figure 2, we display the time evolution of $A^{\max}$, free nucleons, LCPs and IMFs for ^{40}Ca+^{40}Ca reactions respectively at 100 (left panels) and 400 (right panels) MeV/nucleon for central collisions. We see that $A^{\max}$ and free nucleons follow similar behaviour as reported for the reactions of ^{12}C+^{12}C. The emission of free nucleons enhances with the cut and thus reducing the number of LCPs and IMFs. Similar effects can be seen for ^{96}Zr+^{96}Zr reaction (not shown here).

In figures 3 and 4, we display the impact parameter dependence of $A^{\max}$, free nucleons, light charged particles (LCPs) and intermediate mass fragments (IMFs) for the ^{40}Ca+^{40}Ca and ^{96}Zr+^{96}Zr reactions, respectively, at 100 (left panels) and 400 (right panels) MeV/nucleon. From both figures we see that $A^{\max}$ rises uniformly with impact parameter for both methods. The difference increases with impact parameter. This happens because we have a bigger spectator matter (from where $A^{\max}$ generates) at peripheral collision geometry. The number of free nucleons decreases with the increase in impact parameter for both methods.

The emission of fragments in MSTP method shows that in contrast to central collisions, peripheral collisions do not show drastic changes because with increase in colliding

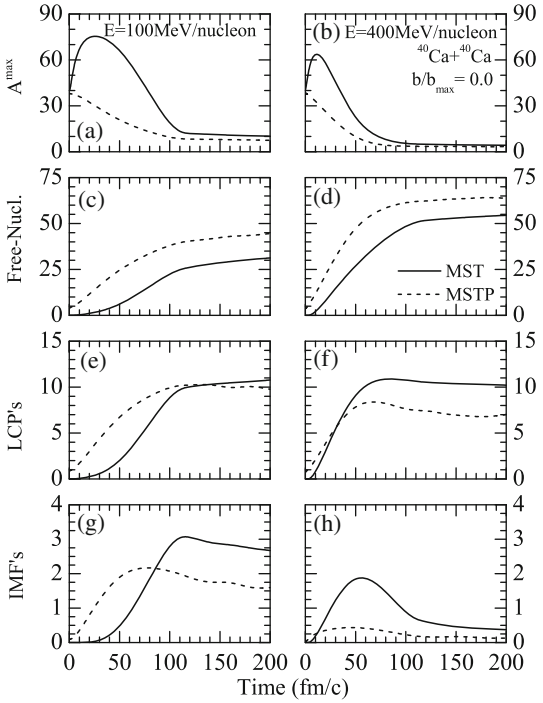

Figure 2. Same as figure 1 but for the ^{40}Ca+^{40}Ca reaction.

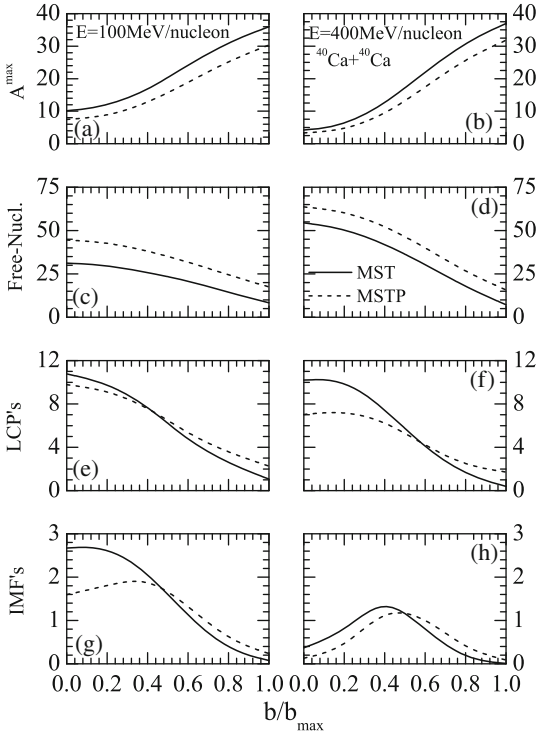

Figure 3. The impact parameter dependence of $A^{\max}$, free nucleons, LCPs and IMFs for the ^{40}Ca+^{40}Ca reaction at 100 (left panels) and 400 (right panels) MeV/nucleon with MST and MSTP methods.

geometry, the fragments are the remnants of either the projectile or the target. Therefore breaking mechanisms are almost bound and therefore MSTP method does not give different results.

In figure 5, we display the impact parameter dependence of $A^{\max}$, free nucleons and LCPs for the ^{12}C+^{12}C reaction at 100 (left panels) and 400 (right panels) MeV/nucleon. From the figure, we see that the effect of momentum cut on $A^{\max}$ follows a similar behaviour with impact parameter as for medium and heavy mass systems, though the role of momentum cut on fragment production changes with impact parameter. We see that in this particular case, the effect of momentum cut on the fragment production enhances with impact parameter (see figures 5e and 5f) which is quite different from the earlier figures (for ^{40}Ca+^{40}Ca and ^{96}Zr+^{96}Zr). This is because the spectator matter even at peripheral geometries will be very less in such a lighter system and so the fragments are emitted mostly from the participant region, where they are unstable and hence momentum cut plays a role at such geometries. Thus, we see that for lighter systems like ^{12}C+^{12}C, the role of momentum cut on fragment production increases with colliding geometry whereas for medium and heavy mass systems, the role of momentum cut on fragment production decreases as one goes to peripheral collisions.

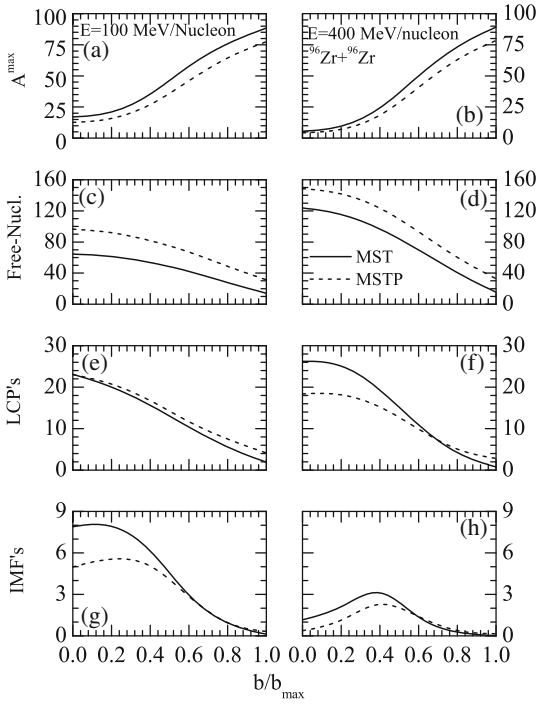

Figure 4. Same as figure 3 but for the ^{96}Zr+^{96}Zr reaction.

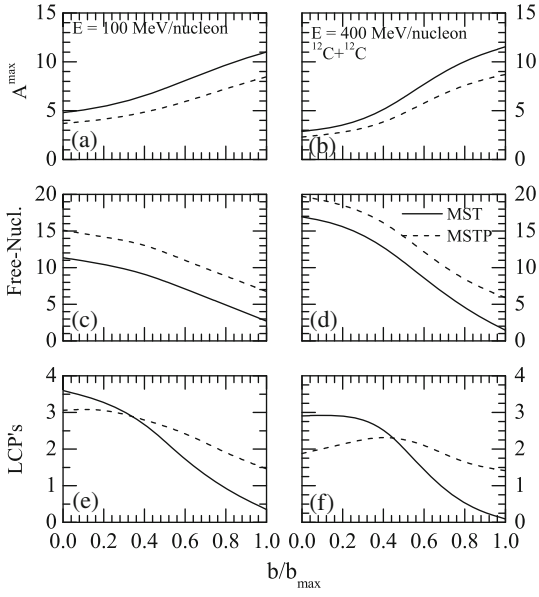

Figure 5. Same as figure 3 but for the ^{12}C+^{12}C reaction.

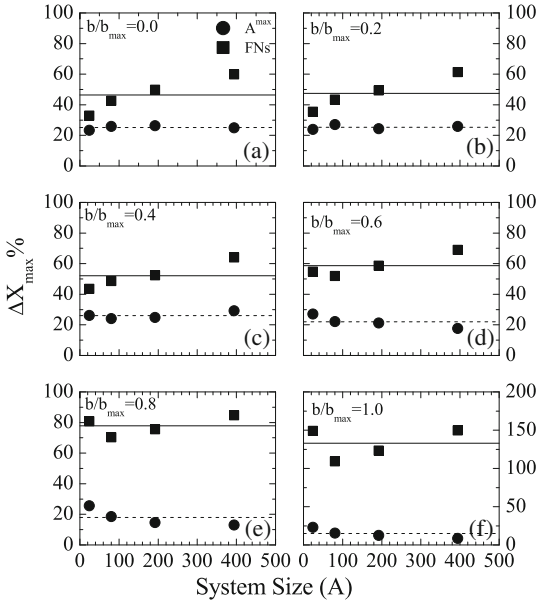

Figure 6. The system size dependence of the percentage difference of $A^{\max}$ and free nucleons between MST and MSTP at various impact parameters at 100 MeV/nucleon. Lines represent the average values.

In figure 6, we display the percentage difference $[(\Delta X(\%) = (X_{(\mathrm{MST})} - X_{(\mathrm{MSTP})}/X_{\mathrm{MST}}) \times 100)]$. We display the system size dependence of the percentage difference of the quantities $A^{\max}$ and free nucleons at $\hat{b} = 0.0, 0.2, 0.4, 0.6$ and 0.8 at an incident energy of 100 MeV/nucleon. We see that percentage difference of $A^{\max}$ (circles) is almost constant and remains independent of the system size at central and semicentral colliding geometries where it is more for lighter systems at peripheral colliding geometries. Similar behaviour is also observed for the free nucleons.

In figure 7, we display the system size dependence of the percentage difference of LCPs and IMFs at various impact parameters at an incident energy of 100 MeV/nucleon. From the figure we see that in central collision, ΔIMF% is almost independent of the system size whereas at peripheral colliding geometries it increases with system mass. The average difference is 22, 69, -45 and -16 for $A^{\max}$, free nucleons, LCPs and IMFs, respectively.

As a last step, we also compare our calculations with the experimental data. Since there is no available data till date on systems as light as ^{12}C+^{12}C, we chose ^{197}Au+^{197}Au reaction. In figure 8, we display the charge distribution for ^{197}Au+^{197}Au reaction at 150 (left panels) and 250 (right panels) MeV/nucleon at central ($b = 0$–3.5) and semicentral ($b = 0$–8) colliding geometries. The data are taken from refs [13–15]. Solid (open) circles represent the results for MST (MSTP) method. From the figure, we see that both MST and MSTP methods obey the qualitative behaviour of charge distribution, though, quantitatively, MST overpredicts the data at both the energies and both colliding geometries.

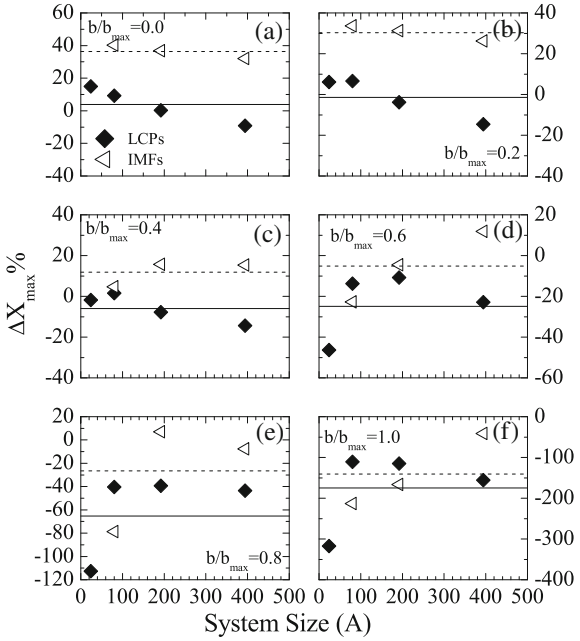

Figure 7. Same as figure 6, but for the LCPs and IMFs.

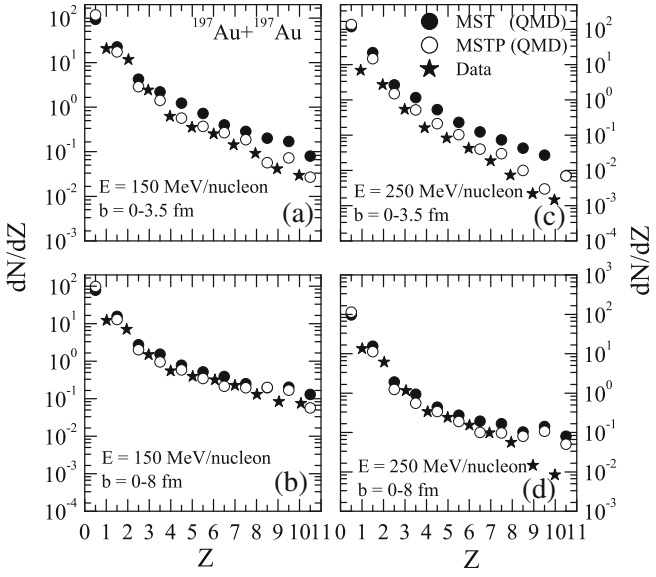

Figure 8. Charge distribution for central and semicentral reactions of ^{197}Au+^{197}Au reactions. The experimental values for the central collisions at 150 MeV/nucleon are taken from ref. [13] whereas the ones for the semicentral collisions at 150 MeV/nculeon are taken from ref. [14]. All experimental data for collisions at 250 MeV/nucleon are taken from ref. [15]. Circles represent our theoretical calculations.

On the other hand, we find that MSTP method matches the data well at both energies and colliding geometries.

Using quantum molecular dynamic model, we studied the role of momentum correlations in fragmentation. This was achieved by imposing cut in momentum space during the process of clusterization. We find that this cut yields significant difference in the multifragmentations of the system at all colliding geometries. The study also pointed towards a better agreement of the experimental data with the momentum cut.

Acknowledgements

This work is done under the supervision of Dr Rajeev K Puri, Department of Physics, Panjab University, Chandigarh, India. This work is supported by a grant from the Centre of Scientific and Industrial Research (CSIR), Govt. of India.

References

[1] M Begemann-Blaich, *Phys. Rev.* **C48**, 610 (1993)
M B Tsang *et al*, *Phys. Rev. Lett.* **71**, 1502 (1993)
D R Bowmann *et al*, *Phys. Rev. Lett.* **67**, 1527 (1991)
W Reisdorf *et al*, *Nucl. Phys.* **A612**, 493 (1997)
W Bauer, G F Bertsch and H Schulz, *Phys. Rev. Lett.* **69**, 1888 (1992)
[2] J Aichelin, *Phys. Rep.* **202**, 233 (1991)
[3] J Singh, S Kumar and R K Puri, *Phys. Rev.* **C62**, 044617 (2000)
Y K Vermani and R K Puri, *Europhys. Lett.* **85**, 62001 (2009)
[4] C Dorso and J Randrup, *Phys. Lett.* **B301**, 328 (1993)
[5] J Singh and R K Puri, *J. Phys. G: Nucl. Part. Phys.* **27**, 2091 (2001); *ibid*, *Phys. Rev.* **C62**, 054602 (2000)
[6] S Kumar and R K Puri, *Phys. Rev.* **C78**, 064602 (2008); *ibid*, **C58**, 320 (1998); *ibid*, **C57**, 2744 (1998)
[7] R Chugh *et al*, *Phys. Rev.* **C82**, 014603 (2010)
S Gautam *et al*, *J. Phys. G: Nucl. Part. Phys.* **37**, 085102 (2010); *ibid*, *Phys. Rev.* **C83**, 014603 (2011)
[8] S Kumar *et al*, *Phys. Rev.* **C81**, 014601 (2010); *ibid*, **C81**, 014611 (2010)
V Kaur *et al*, *Phys. Lett.* **B697**, 512 (2011)
[9] J Dhawan *et al*, *Phys. Rev.* **C74**, 057901 (2006); *ibid*, **C74**, 057610 (2006)
[10] C Fuchs *et al*, *J. Phys. G: Nucl. Part. Phys.* **22**, 131 (1996)
Y K Vermani *et al*, *Nucl. Phys.* **A847**, 243 (2010)
G Batko *et al*, *J. Phys. G: Nucl. Part. Phys.* **20**, 461 (1994)
S W Huang *et al*, *Prog. Part. Phys.* **30**, 105 (2003)
[11] E Lehmann *et al*, *Phys. Rev.* **C51**, 2113 (1995); *ibid*, *Prog. Part. Nucl. Phys.* **30**, 219 (1993)
[12] J Cugnon, T Mizutani and J Vandermeulen, *Nucl. Phys.* **A352**, 505 (1982)
[13] FOPI Collaboration: C Kuhn, *Phys. Rev.* **C48**, 1232 (1993)
[14] Th Wienold, *Fragment production and collective flow behaviour in central* $^{197}Au+^{197}Au$ *reactions at* $E/A = 100$ *MeV to 800 MeV*, Ph.D. thesis (University of Heidelberg, 1993), GSI report, GSI-93-28, ISSN 0171-4546
[15] U Sodan, Ph.D. thesis (University of Heidelberg, 1994) (unpublished)